Proceedings of the 25th International Conference on
Port and Ocean Engineering under Arctic Conditions
June 9-13, 2019, Delft, The Netherlands

An approach to establish sea ice design load cases south of the Barents Sea polar front

Edmond Hansen[1], Juliane Borge[1], Martin Arntsen[1], Nicolas Serre[1], Åse Ervik[1], Trine Lundamo[1], Mark Thomson[2], Andreas Olsson[2]

[1] Multiconsult (Tromsø, Norway)
[2] OMV Norge AS (Stavanger, Norway)

ABSTRACT

An approach for deriving sea ice design load cases (DLCs) during rare intrusions of sea ice at the Wisting oil and gas field in the northwestern Barents Sea is described. The DLCs are combinations of sea ice parameter values likely to cause global loads at selected return periods. Wisting is located only ~100 km south of the Barents Sea polar front, which separates cold water at freezing from warmer water south of the front. Historically, sea ice has occurred south of Wisting. However, there are no recent (since 1978) occurrences. Sea ice occurrence probability is calculated through extreme value statistics, but the sea ice characteristics cannot be extrapolated in the same way. Moreover, precise numerical mooring load calculations in broken ice conditions are prohibitively time consuming. An approach to calculate DLCs was devised, involving 1) estimation of statistical characteristics of the sea ice parameters from existing data/literature upstream from Wisting, 2) transformation of the parameter values to the Wisting location, 3) statistical simulation of simultaneous long time series (100 000 years) of all parameters, 4) assessment of the combined effect of the parameters through analytical computation of an ice severity index, as function of the relevant sea ice parameters, and 5) determination of ice severity index values at selected return periods. The corresponding values of sea ice parameters are selected to form a set of DLCs at Wisting, subsequently used in ice tank tests and in numerical simulations to calculate global sea ice loads.

KEY WORDS: Sea ice; Design load; Barents Sea; Load index; Metocean.

INTRODUCTION

The occurrence of sea ice is a major driver for the design and operation of concepts for exploitation of oil and gas in the northern Barents Sea. The probability of sea ice occurrence influences the choice of concept, while the corresponding sea ice loads influences its design.

The western Barents Sea features a seasonal sea ice cover, typically extending south to the

topographically controlled Polar front. The front is located approximately 90-120 km north of the northernmost oil field presently under development in the Norwegian sector, Wisting (73° 30' N, 024° 14' E). During winter, the Polar front separates cold and relatively fresh water at freezing temperature in the north from warmer and more saline water well above freezing in the south. Persistent northerly winds may drive sea ice south of the front. On longer time scales, the southward sea ice extent is strongly correlated with the inflowing Atlantic heat (Årthun et al., 2012).

Historically, sea ice has occurred well south of Wisting (Divine and Dick, 2006; Vinje, 2001). However, during the recent period in which consistent ice extent observations are available from remote sensing (1978-present, SSMR/SSMI passive microwave), sea ice never occurred at Wisting itself. The shortest distance from Wisting to the ice edge observed since 1978 is 21 km (Multiconsult, 2018b). Sea ice nevertheless shows up at Wisting in the extreme value statistics, at probability levels requiring design for sea ice (ISO 19906, Norsok N003).

The challenge is then to quantify the characteristics of the ice, such as thickness, typical concentrations, floe sizes, ridge frequency, keel depth, and so forth, during events of ice occurrence at Wisting. Existing data from the region quantify the characteristics of sea ice in low water temperatures north of the Polar front. In the event of sea ice intrusions on oil fields south of the Polar front, the characteristics are likely to change significantly during the drift southwards over relatively warm water. Moreover, the goal is to derive sea ice design load cases, i.e. combinations of the sea ice parameters governing the resulting ice actions and loads. This implies identifying combinations of the parameters occurring at selected annual exceedance probabilities.

In this study, we present an approach to define sea ice design load cases at Wisting. The approach combines extrapolation of upstream measurements of ice properties and statistical simulation of simultaneous long term time series of all parameters (100 000 years, ensuring ability to handle also 10^{-5} ALARP considerations). The long time series is used in conjunction with a simplified ice severity index to identify events of high global sea ice loads. The result is a set of combinations of sea ice parameters, occurring at selected return periods and yielding the highest global loads. These combinations of ice characteristics should subsequently be used in ice tank tests and in numerical simulations to calculate global sea ice loads.

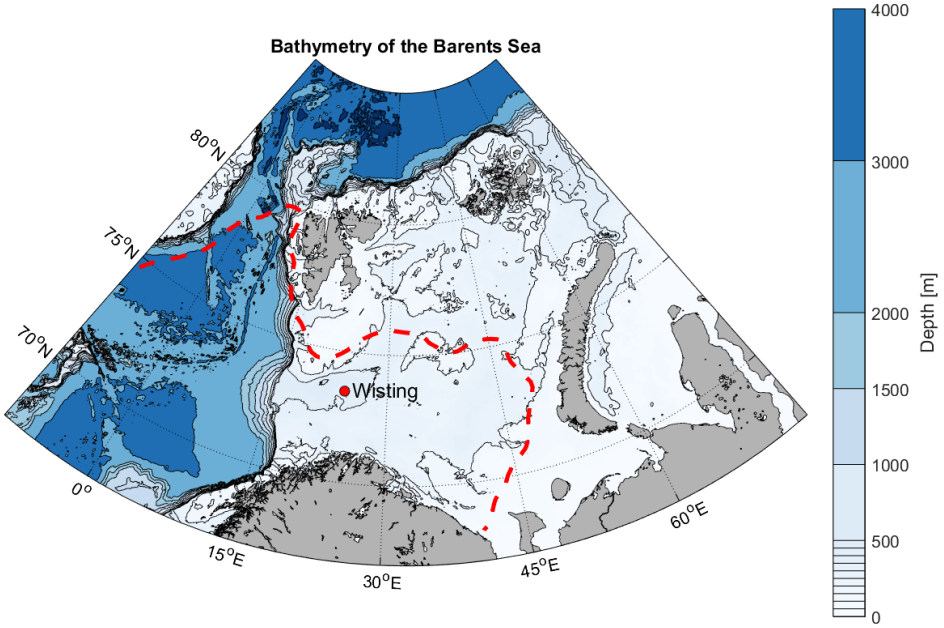

Figure 1 The location of Wisting in the northwestern Barents sea. The red dashed line draws a line where sea ice with concentration above 0.15 occurred 30% of the April months during the 1985-2014 period (the ice edge definition in the public management plan for the region).

DATA AND METHODS

Sea ice parameters at Wisting

The parameters considered in this study are concentration, floe size, level ice thickness, level ice mechanical properties, and the ridge frequency, rubble thickness, consolidated layer thickness, and rubble porosity. The distance to the ice edge is also a central parameter.

There are no observations of sea ice at Wisting. The values of the selected sea ice parameters must be taken from relevant upstream observations (north of the polar front), and extrapolated/transformed to Wisting (ISO19906:2010). In the following, this process is briefly outlined (the full details are provided in a technical report (Multiconsult, 2018a)).

The distance from Wisting to the ice edge was calculated from 1978-present passive microwave (SSMR/SSMI; available from nsidc.org) daily ice concentration charts. Here the ice edge is defined as concentration 0.1, which is slightly more conservative than the definition of the public management plan (Figure 1). This parameter was never zero (i.e., ice at Wisting), but its distribution enables extrapolation and extreme value statistics to be carried out. The return period of sea ice at Wisting (distance is zero) is approximately 100 years (Multiconsult, 2018b). Negative distances mean that Wisting is within the ice. The data was used to simulate sea ice occurrence events.

Sea ice occurring at Wisting is likely to drift in from the north, from the cold water at freezing temperatures north of the polar front. Such sea ice will melt during its passage from the polar front to Wisting, a distance of 90-120 km across seawater well above freezing temperatures. Assumptions must be made regarding the oceanic heat fluxes available to melt the ice. It is a central assumption that a lower estimate (100 W/m^2) is taken from the range available from literature. This represents a situation where persistent northerly winds push new sea ice south across the polar front, continuously building on a freshwater layer beneath the ice from melting ice. The layer of cold freshwater insulates the sea ice from the warmer water further below, thereby reducing the oceanic heat fluxes.

Under such conditions, a 200 km wide marginal ice zone (MIZ) is assumed (the assessment is based on relevant ice charts from met.no, i.e., charts during periods of northerly winds). The average sea ice concentration is quantified by a curve fit as a function of the distance from Wisting to the ice edge, based on ice charts from met.no and observations (Løset et al., 1997; Gherardi and Lagomarsino, 2015). A concentration of 1.0 is assumed at the inner border of the MIZ. The mean ice floe size was quantified in a similar way, as a function of distance to the ice edge, based on observations (Løset et al., 1997; Gherardi and Lagomarsino, 2015). The mean floe size – with its dependence to the distance to the ice edge – is used to characterize a floe size distribution. Based on three data sets in Gherardi and Lagomarsino (2015), the governing parameters in the floe size distribution function is established, as function of the mean floe size. In essence, the floe size distribution is then also a function of the distance to the ice edge. For further details regarding this approach, we refer to Multiconsult (2018a).

The level ice thickness is deduced from ice draft observations by upward looking sonars in the Olga Basin from 1995/96 (Abrahamsen et al., 2006). Due to the many sources of uncertainty, the draft is bluntly used as thickness. With the original thickness series available, level ice at different thicknesses could have been separated from deformed ice. However, only the digitized ice thickness distribution was available for our analysis. Following Hansen et al. (2014), estimates of the proportions of deformed and level ice were established from the distribution. The inflection point of the modal peak is taken as the transition from predominantly level ice to ridged ice. However, thin deformed ice exists below this transition point. The proportion of deformed ice below the inflection point is taken (Hansen et al., 2014) to increase linearly from 0% at 0 m draft, to 100% at the inflection point. This provides thickness distributions for level and deformed ice (Figure 2).

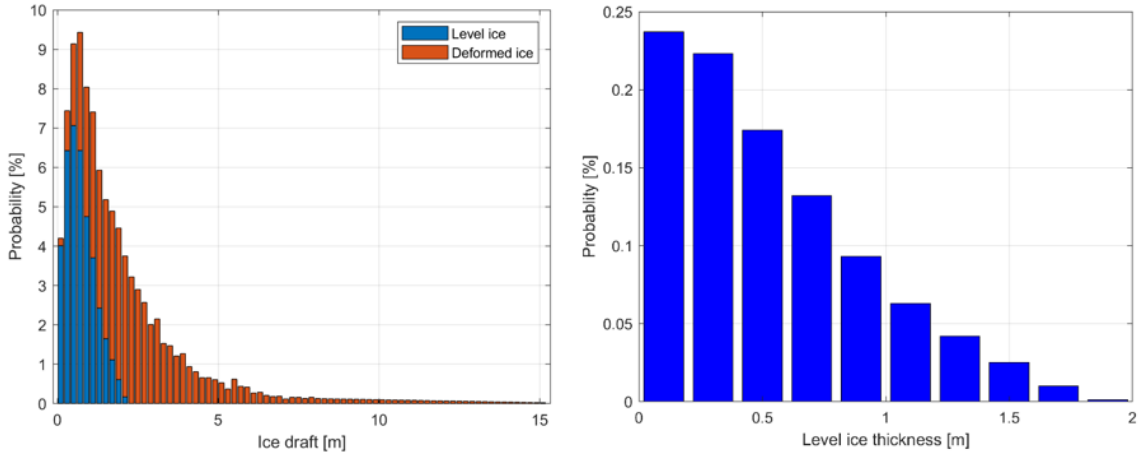

Figure 2. Left panel: ice draft/thickness, and the partition into thickness distributions for level and deformed ice. Right panel: resulting thickness distribution of level ice at Wisting.

With the assumed oceanic heat of 100 W/m^2, the distance from the polar front to Wisting of 90-120 km, and drift speeds of 0.1 and 0.2 m/s, the average melt of level ice is calculated to ~0.35 m. The resulting thickness distribution of level ice is seen in the right panel of Figure 2. When constructing the long time series, level ice thicknesses are found by drawing from this distribution.

The ridge frequency distribution is based on data from the Barents Sea west of 35° E (Vinje (1984), approximately 1700 ice ridge measurements). We assume that the majority of the measurements are performed in ice with high concentration (close to 1) and that the ridge frequency is proportional to the ice concentration. Therefore, in the long time series, the ridge frequency at each time step is calculated by drawing from the empirical distribution from Vinje (1984), and multiplying by the ice concentration in that time step.

The consolidated layer thickness is calculated from the level ice thickness drawn from the distribution in Figure 2 (right panel), where the melted level ice is added (0.35 m) and the resulting thickness is multiplied by 1.6 (ISO19906:2010). This assumption means that the consolidated layer is proportional to the level ice thickness before melting, and introduces a correlation.

The rubble thickness was estimated along the same lines as the level ice thickness. The draft distribution of the deformed ice in Figure 2 was used, but melted using an oceanic heat flux of 300 W/m^2 (an assumption made due to deeper penetration into the stratified ocean than level ice), and taking the macro-porosity of the rubble into account. This results in a general subtraction of 1.5 m of estimated ice rubble melt at Wisting. In addition, an estimated mean consolidated layer (1.4 m) was subtracted from the ice keel draft to obtain the ice rubble thickness. This number is a result from the relationship with level ice and the statistical simulations (see above). This is an approximation due to the unknown relationship between the ice keel and consolidated layer thicknesses, especially in decaying ice. The ice ridge sail is not included in the ice severity index and is therefore not included here.

The values of the level ice and ridge mechanical properties were generally taken from available literature, summarized in Table 1. The selection is based on judgement, and is consistent with recommendations in ISO19906:2010.

Table 1 Mechanical properties of level ice (above separation line) and ice ridges (below separation line).

Ice property	Unit	Value	Distribution
Ice density	kg/m^3	900-920	Uniform
Elastic modulus	GPa	1.0-2.0	Uniform
Poisons ratio	-	0.3	Constant
Uniaxial compressive strength	MPa	0.8-1.6	Uniform
Flexural strength	kPa	200-400	Uniform
Rubble porosity	-	0.1-0.3	Uniform
Internal friction angle	-	20°-40°	Unifrom
Rubble cohesion	kPa	5-7	Uniform

Ice severity index

An *ice severity index* is introduced as a way to assess the combined contribution from each ice parameter to the global load. It is quantified as an *equivalent level ice thickness* - ELI (Keinonen et al.,1996, 1998). This approach allows handling of a complex sea ice environment with a single parameter. The number of load contributing parameters is reduced to one, which is used to assess the severity of the ice conditions, i.e., combinations of ice parameters. The global ice load on the structure is related to the equivalent level ice thickness. An ELI with a specific return period, corresponds to an ice condition (parameter combination) severity with the same return period. Here, it is to be understood as an *ice severity index*, expressed as (Keinonen et al.,1996, 1998)

$$ice\ severity\ index = H_{ice} \cdot C_{Concentration} \cdot C_{FloeSize} \cdot C_{strength}, \quad (1)$$

where H_{ice} represents the effects from ice thickness and ice ridges, $C_{Concentration}$ represents the effects from ice concentration, $C_{FloeSize}$ represents the effects from the ice floe size, and $C_{strength}$ represent the effects from the ice strength. Keinonen et al. (1996, 1998) derived empirical expressions for these coefficients from icebreaker data with measurements of thruster propulsion and expert judgement. The relevance of using this methodology for our purpose is discussed in the Discussion section. In the following we outline which parameters contribute to the coefficients in the ice severity index. For a full technical description, we refer to the original works of Keinonen and co-authors.

The ice thickness and ice ridge coefficient H_{ice} is a function of level ice thickness, consolidated layer thickness, ridge width, macro porosity, rubble thickness and ridge density (number per meter) (Keinonen et al.,1996, 1998). The ridge width w is expressed as a function of the ridge keel depth, following Timco and Burden (1997).

The ice concentration coefficient $C_{Concentration}$ is expressed as the cube of the concentration (ranging from 0 to 1). This is a modification of the orginal model of Keinonen et al. (1996, 1998), introduced to ensure a continuous equation at low concentrations. Our modified model and the original of Keinonen et al. (1996, 1998) are plotted jointly in Figure 3 a).

The ice floe size coefficient $C_{FloeSize}$ is expressed through a logarithmic functional relation to the floe size. In this study the mean floe size is used as input. The mean floe size is calculated from the number of floes. However, in a broken ice field it is likely that the largest global ice actions are imposed by the largest floes. It is intuitive that using a larger floe size within the ice floe size distribution of a specific ice field would give a more conservative representation of the ice field action. Work is ongoing to address the effect of rather using the 90th percentile floe size, calculated from the floe areas, to calculate $C_{FloeSize}$.

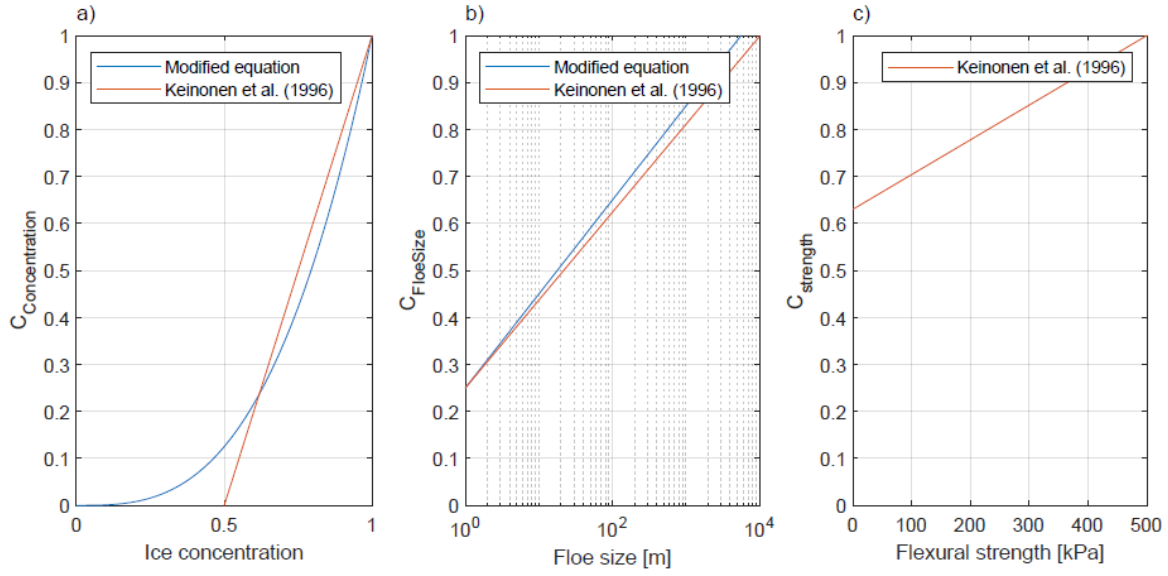

Figure 3. The ice severity index coefficients a) $C_{concentration}$ = f(concentration), b) $C_{FloeSize}$ = f(floe size), and c) $C_{strength}$ = f(flexural strength).

The ice floe size coefficient of Keinonen et al. (1996, 1998) was slightly modified for our purpose. In the original model equation, $C_{FloeSize}$ reaches its maximum value at a floe size of 10 000 m (see model curve in Figure 4b). In our study, a limit of 5500 m is used, based on a limit momentum calculation (Sodhi, 2003), assuming an ice drift speed of 0.2 m/s, a compressive strength of 1100 kPa, and a structure of width 55 m. The modified model is plotted jointly with the original Keinonen-model in Figure *3*b.

The ice strength coefficient $C_{strength}$ is a linear relation with the flexural strength (Keinonen et al., 1996, 1998). It is shown in Figure *3*c).

Statistical simulation of long time series

Based on the derived statistical characteristics of the sea ice parameters, long time series of the sea ice parameters are simulated with probabilistic methods. The relationships between the parameters in the probabilistic model are displayed in Figure 4. Sea ice concentration and ice floe size are assumed to be in functional relationship with the distance to the ice edge, while the other parameters only depend on whether sea ice occurs or not. The consolidated layer thickness is a function of the level ice thickness, while the ridge frequency is linked to the ice concentration. Ideally, the probabilistic model should include more relationships between the parameters. However, as sea ice never was observed at Wisting, there is considerable uncertainty associated with the parameters and their intercorrelations.

The methods used to generate the different parameters of the synthetic time series are listed in Table 2. A time series of 100 000 years lengths with time step one day is generated. The ice severity index is calculated for the whole time series. The return level of ice severity index for return periods of 100 years and 10 000 years is estimated. The time steps with values of ice severity index closest to the obtained return levels are identified in order to extract the resulting parameter combinations constituting the DLCs.

Distance to ice edge

In order to generate a long time series of distance to the ice edge the following steps were followed

1. For each year: Find the annual number of events with distances below 160 km by drawing from a Poisson distribution.
2. For each event: Find the minimum distance within each event by drawing from an exponential distribution.
3. For each event with minimum distance below 0 km (sea ice at Wisting):
    a. Find the length of each event by assuming ice drifting from 0 km distance to the minimum distance and back with a drift speed given by a normal distribution (with mean 0.2 m/s, std=0.1 m/s, lower bound 0.1, upper bound 0.5).
    b. Define distances to the ice edge for the other times in each event by assuming a triangle shape for events of 3 days duration or more, for 3 days starting at 0.1 km inside the ice, for longer periods starting from a random point between 0 and 10 km within the ice.
4. Uniformly distribute the periods throughout the year. Seasonality is not taken into account.

The resulting long term time series of distances from the ice edge to Wisting defines sea ice occurrence (distance below 0 km) and serves as basis for determination of floe size distribution and ice concentration.

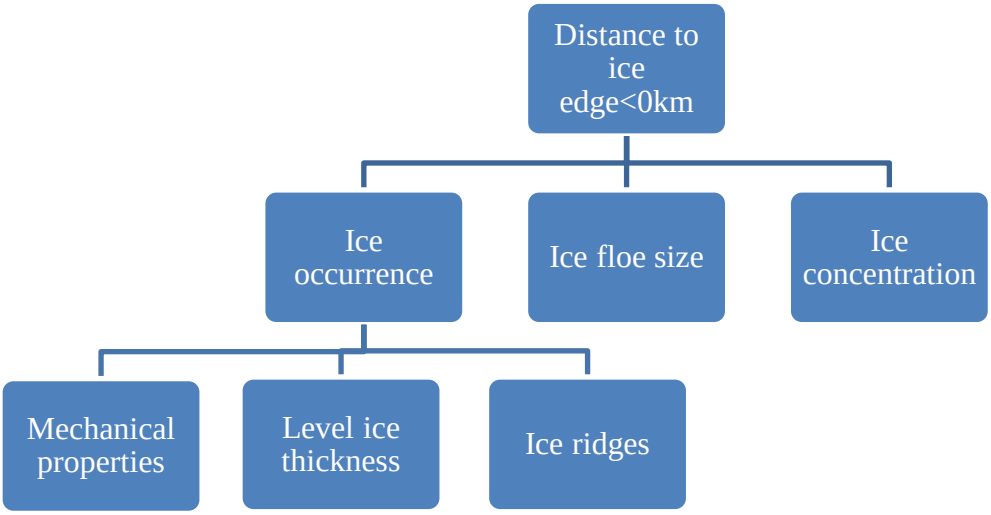

Figure 4. Diagram showing the relation between the parameters in the probabilistic model. For example, ice thickness only depends on ice occurrence, while ice concentration depends on distance to the ice edge.

Table 2. Methods used in the probabilistic model

Parameter	Method
Distance to ice edge	As outlined in text above ("Distance to ice edge")
Ice occurrence	If distance to ice edge is below 0
Ice concentration	Empirical function of distance to ice edge
Mean ice floe size	Empirical function of distance to ice edge
Level ice thickness	Draw from empirical distribution
Ridge frequency	Draw from empirical distribution + function of concentration
Consolidated layer thickness	Function of level ice thickness
Rubble Thickness	Draw from empirical distribution
Mechanical properties	Draw from parametric distribution

RESULTS

A method to establish sea ice design load cases (DLCs) has been described. In terms of this paper, the main result is the method itself. It enables us to define DLCs for given return periods, at a site where no data on sea ice characteristics exists. The method is a pragmatic approach, with inherent weaknesses discussed in the next section. It nevertheless provides a set of sea ice DLCs, which are used at a later stage to address global loads in ice tank tests and by numerical modeling.

In this context, the resulting distribution of sea ice characteristics and set of DLCs at Wisting are less relevant. Some of the preliminary key findings are nevertheless listed in the following. It provides an example of the outcome of the method, and the experienced reader – familiar with the governing physics of the northwestern Barents Sea - may use the numbers to gauge the validity of the approach.

Sea ice intrusions at Wisting occur with a return period of approximately 100 years. During these rare events, Wisting is approximately 20 km within the ice, on average. During the 100 000 year long synthetic time series, very rare events occurred where Wisting was up to 200 km within the ice. The concentration is 0.45 during the ice intrusions, on average. The corresponding mean floe size is 58 m (calculated from number of ice floes, not from their area). The mean level ice thickness is 0.5 m, while the mean ridge frequency is 5 per km.

This listing of values for some of the ice parameters, provide a univariate impression of the average values. However, any summary statistic from the individual distributions is of limited use when the overall ice condition should be assessed. This is where the ice severity index comes into use. Based on the long synthetic time series of the individual parameters, a time series of the ice severity index was calculated. Values of the index at given (low) annual exceedance probabilities, point to combinations of ice parameters constituting severe ice conditions. At the timestep where these rare index values occur, the corresponding values of the underlying ice parameters are extracted. Each of these set of ice parameters is then used to characterize the ice conditions that stand out as severe at a certain return period. Each set of combinations constitutes a DLC.

An example list of DLCs is shown in Table 3. In each parameter combination, one or more parameters contribute particularly much to the high value of the ice severity index. In Table 3, the parameters contributing most to the ice severity is marked with orange background. Each DLC is associated with a return period, or annual probability of exceedance. It is observed how the different parameters balance each other to yield a severe ice condition: The level ice thickness may be low, but high values of rubble thickness or consolidated layer thickness

contribute to the severity of the ice condition, and vice versa. The most severe conditions are rare (low annual probability of exceedance), with concurrent high values of several of the parameters. The central reason for taking this whole approach into use, is that this selection of combinations is objective and based on physics and intercorrelations between the parameters, thereby providing statistically plausible combinations. The set of DLCs (only a few are shown here), are then used to set up ice tank tests and perform numerical simulations to calculate the resulting global loads.

Table 3. Sea ice design load cases (DLCs) at two levels of annual probability of exceedance. Each DLC is representing a combination of ice parameters likely to cause design loads. The two rows in italics (marked a and b) are used in an example in the Discussion section. The orange background indicates particularly high values of the parameter.

Annual probability of exceedance	Ice conc.[ ]	Level ice thickness [m]	Mean/P90 ice floe size [m]	Flexural strength [kPa]	Ridge frequency [km^{-1}]	Rubble thickness [m]	Consolidated layer thickness [m]	Keel porosity [ ]
10^{-2}	0.4	1.1	43/511	340	2	7.2	2.4	0.16
	0.6	0.3	62/761	321	1	0.6	1.0	0.26
	0.5	0.4	51/618	294	10	1.1	1.3	0.24
	0.4	0.2	45/544	363	5	10.5	0.9	0.28
10^{-4}	1.0	0.5	155/1695	234	11	10.0	1.4	0.29
a)	*0.9*	*0.9*	*131/1488*	*201*	*17*	*5.7*	*2.1*	*0.25*
b)	*1.0*	*1.6*	*182/1890*	*351*	*7*	*3.4*	*3.1*	*0.13*
	1.0	1.4	182/1890	377	14	2.9	2.8	0.12

DISCUSSION

The approach of using the ice severity index to derive generic DLCs independent of structure shape is imperfect. The index is based on empirical analyses of icebreaker resistance in ice-covered waters at relatively high concentrations. Here it is used to point to severe ice conditions for moored structures of unknown shape, also when the concentration is low.

Generally, many ship shaped floating structures would be relevant to address with the Keinonen approach, as the semi-empirical index is based on a wide range of hull shapes. The relevance for other structures are more questionable. For example, with its origin being ice loads on icebreakers, the index contains a term for flexural strength only. For structures carrying loads imposed through ice crushing, the severity of the ice condition is not fully addressed. Or, in other words, variability in the crushing strength is not taken into account when characterizing the severity of the ice conditions. However, as variability in the crushing strength is largely expected to follow variability in the flexural strength, this is not the greatest point of concern. It is maybe more relevant to look into the sensitivity to the other load driving parameters.

We use the DLCs in Table 3 as an example to illustrate this latter point. Consider the two middle rows for the 10^{-4} annual exceedance probability, marked in italics and labeled a) and b). Of the two combinations, row b) features the highest values of most parameters. They are still at the same probability level, since row a) has significantly higher number of ice ridges. However, the combination of thicker level ice and consolidated layer of row b) could lead to

this combination being a more severe ice condition for a structure with vertical sides. Such sensitivities must be addressed when the loads are calculated.

Due to the lack of data, not all correlations are accounted for. As an example, some DLCs feature very deep pressure ridges despite relatively thin level ice, e.g. row 4 in Table 1.

Nevertheless, given the fundamental lack of data at the site and the unavailability of methods for efficient calculation of global loads in broken ice, the approach provides useful insight. It is important to stress that it does not indicate load levels, or ice-structure interaction scenarios. The approach points to combinations of sea ice parameters that are likely to yield the highest global loads during rare events of sea ice. The value of this approach must be seen in conjunction with subsequent ice tank tests, as well as analytical and numerical global load calculations. Those analyses must address sensitivities and the issues left open following this study.

CONCLUSIONS

This study describes an approach to derive design load cases (DLCs) during rare intrusions of sea ice in the area of the Wisting oil and gas field in the northwestern Barents Sea. The DLCs are combinations of values of sea ice parameters which are likely to cause global loads at selected probabilities of annual exceedance.

There are no sea ice observations at Wisting itself. Sea ice occurrence may readily be calculated through extreme value statistics, but the characteristics of the sea ice cannot be extrapolated in the same way. Moreover, precise numerical load calculations under the various DLCs are prohibitively time consuming. An alternative approach was devised, as outlined below:

1. Estimation of statistical characteristics of the sea ice parameters from existing data/literature upstream from Wisting.
2. Transformation of the parameter values to the Wisting location
3. Statistical simulation of simultaneous long time series (100 000 years) of all parameters.
4. Assessment of the combined effect of the parameters through analytical computation of an ice severity index, as function of the relevant sea ice parameters.
5. From the long term time series of ice severity index, determination of the ice severity index values at selected annual exceedance probabilities.
6. The corresponding values of sea ice parameters are selected to form a set of Design Load Cases for sea ice at Wisting.

REFERENCES

Abrahamsen E. P., Østerhus S. and Gammelsrød T., 2006. Ice draft and current measurements from the north-western Barents Sea, 1993-96, *Polar Research* 25(1), p 25-37

Divine, D. V. and Dick, C., 2006. Historical variability of sea ice edge position in the Nordic Seas. *J. Geophys. Res.*, Vol. 111, C01001, doi:10.1029/2004JC002851.

Gherardi, M. and Lagomarsino, M. C., 2015. Characterizing the size and shape of sea ice floes. *Nature, Scientific Reports,* 5, doi.org/10.1038/srep10226.

Hansen E., Ekeberg O.C., Gerland S. and Tshudi M. A., 2014. Variability in categories of Arctic sea ice in Fram Strait, *J. Geophys. Res: Oceans,* 119, DOI: 10.1002/2014JC010048

ISO19906:2010. Petroleum and Natural Gas Industries – Arctic Offshore Structures. *International Standardization Organization*, Geneva; Switzerland.

Keinonen A., Browne R. and Nevill C., 1996. Icebreaker Characteristics Synthesis. *Report for Transportation Development Centre, Transport Canada.* TP 12812E.

Keinonen A., Browne R. and Nevill C., 1998. Icebreaker Characteristics Synthesis-performance models, seakeeping and icebreaker escort. *Report for Transportation Development Centre, Transport Canada.* TP 12812E-3.

Løset, S., Shkhinek, K., Strass, P., Gudmestad, O. T., Michalenko, E. B. and Kärnä, T., 1997. Ice conditions in the Barents and Kara seas. *In proceedings of the international conference on offshore mechanics and arctic engineering – OMAE1997*, pp. 173–182, Yokohama, Japan, April 13-17, 1997. American society of mechanical engineers.

Multiconsult, 2018a. Wisting – Sea ice design load cases. *Technical report*, 713992-RIMT-RAP-004, November 15, 2018/0.

NORSOK N003:2017, Actions and action effects. Norsk Standard (standard.no).

Multiconsult, 2018b. Wisting – Sea ice occurrence. *Technical report*, 713992-RIMT-RAP-001, September 14 15, 2018/2.

Sodhi D.S. and Haehnel, R.B., 2003. Crushing ice forces on structures. *Journal of Cold Regions Engineering ASCE*, Vol. 17(4), pp. 153-167, https://doi.org/10.1061/(ASCE)0887-381X(2003)17:4(153).

Timco, G. W. and Burden, R.P., 1997. An analysis of the shape of sea ice ridges, *Cold Regions Science and Technology*, Vol. 25(1), pp 65-77, https://doi.org/10.1016/S0165-232X(96)00017-1.

Vinje, T., 1984. Frequency distribution of sea ice, ridges and water openings in the Greenland and Barents Seas – a preliminary report on the "Birds Eye" observations, *Norsk Polarinstitutt Rapportserie, Report no. 15,* 1984, Norwegian Polar Institute.

Vinje, T., 2001, Anomalies and trends of sea-ice extent and atmospheric circulation in the Nordic Sea during the period 1864-1998, *J. Climate*, Vol. 14, pp. 255-267, https://doi.org/10.1175/1520-0442(2001)014<0255:AATOSI>2.0.CO;2.

Årthun, M., Eldevik, T., Smedsrud, L. H., Skagseth, Ø., and Ingvaldsen, R. B., 2012. Quantifying the influence of Atlantic heat on Barents Sea ice variability and retreat. *J. Climate*, Vol 25, pp. 4736-4743, DOI: 10.1175/JCLI-D-11-00466.1.